2. Rayleigh Backscattering Noise Modeling: Coherent and Incoherent Crosstalk

The insatiable demand for more data-intensive services like video on demand (VOD), high definition television (HDTV), high speed internet, video conferencing and online gaming has prompted the move towards higher SE systems. For this reason, recent research has focused on the design and feasibility of UDWDM systems with adjacent co-propagating channel spacing less than 50 GHz apart [1-3]. Due to added impairments such as FWM, XGM and coherent crosstalk [1, 3, 4], a lower limit is placed on the achievable unidirectional channel spacing. As an alternative, IB networks have been proposed which promise a doubling of the total throughput of a single fiber. In additional to capacity doubling and limiting of crosstalk between co-propagating channels, IB networks also offer potential benefits in terms of hardware efficiency, network control, maintenance and security.

In this chapter, a channel model is described which is used to analyze the impact of RB noise in IB links. The primary goal is to elucidate the various design tradeoffs regarding the modeling and mitigation of RB noise in IB links and how these tradeoffs affect the achievable channel packing density, choice of modulation format and achievable distance. Two RB noise models will be described: an analytic model

and a numerical model. The performance of both models will be analyzed and compared to experimental results at 10 Gb/s.

2.1 Modeling a Noisy Optical Channel

In this thesis, binary intensity modulated optical links with direct detection (IM-DD) are analyzed due to their widespread deployment and economic feasibility. Alternative coherent and differential modulation schemes will not be considered. The channel model describing the generalized bidirectional network is shown in Fig. 2.1. In this model, two transmitters send optical data in opposite directions down a single fiber. The W-E traveling signal, λ_{WE}, is corrupted by RB noise which is generated by the counter-propagating E-W signal, λ_{EW}. After optical preamplification, additive ASE further corrupts the signal. An optical band pass filter (OBPF) is placed after the amplifier to simulate the effect of an optical demux and removes out of band ASE and RB noise. The optically filtered signal, RB and ASE are detected using a PIN photodiode converting the optical intensity to electrical photocurrent. The electrical signal is then passed through a low pass filter (LPF) to remove out of band noise and a decision circuit detects the binary data.

The critical distinction of RB noise is that it is *colored* while ASE and electrical noise (i.e. thermal and shot noise) are *white*. The consequence of this difference is twofold. First, the impact on the optimal filter (both electrical and optical) design in RB-dominated link will differ greatly from links dominated by white noise. Second, design rules will vary significantly depending on whether the RB noise overlaps in frequency with the signal ($\lambda_{WE} = \lambda_{EW}$) or if the RB noise is separated in

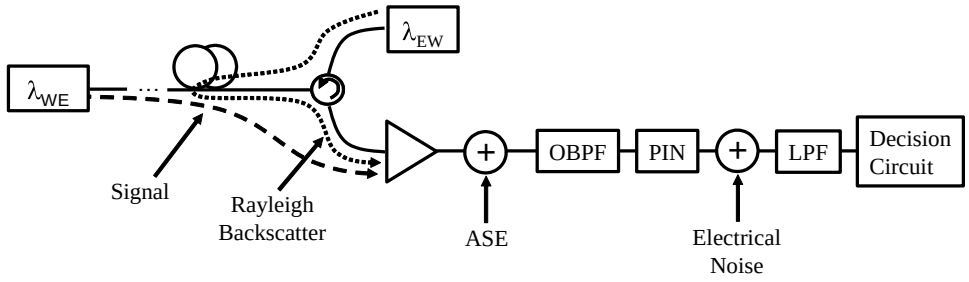

Fig. 2.1. Conceptual schematic of the system under investigation. The W-E signal is detected in the presence of RB noise generated from the E-W signal. Three types of noise are always present in the studied system: ASE, RB and electrical noise from the detection circuitry.

frequency from the signal ($\lambda_{WE} \neq \lambda_{EW}$). By convention, worst case overlapping RB noise will be called *coherent* RB crosstalk while partially overlapping RB noise will be called *incoherent* RB crosstalk.[1] The general case of arbitrarily offset RB and signal is illustrated in Fig. 2.2. From Fig. 2.2, it is clear that optical and electrical filtering can reject a portion of the RB, ASE and electrical noise. As the frequency offset (Δf) between counter-propagating channels decreases, however, larger amounts of RB noise will pass to the decision circuit resulting in a higher probability of bit errors. Therefore, a balance must be determined which maximizes the channel density for optimal capacity while also minimizing the amount of unfiltered noise which passes to the decision circuit. To optimize this tradeoff, the noise variances

[1] To clarify, the term coherent crosstalk does *not* imply that the signal and noise fields are *mutually coherent* but rather that they share a common carrier frequency. Based on physical considerations developed in Appendix I, the phase of the RB field and signal field are always statistically independent in practical situations and thus interference cross-terms average to zero. Even in the case that coherent RB crosstalk is generated by the same laser, coherence times of the laser field tend to be sufficiently small compared to overall path delays such that the signal and RB electric fields can be treated as mutually incoherent. In this thesis, phase relationships between the signal and RB field will be assumed to be uncorrelated and statistically independent.

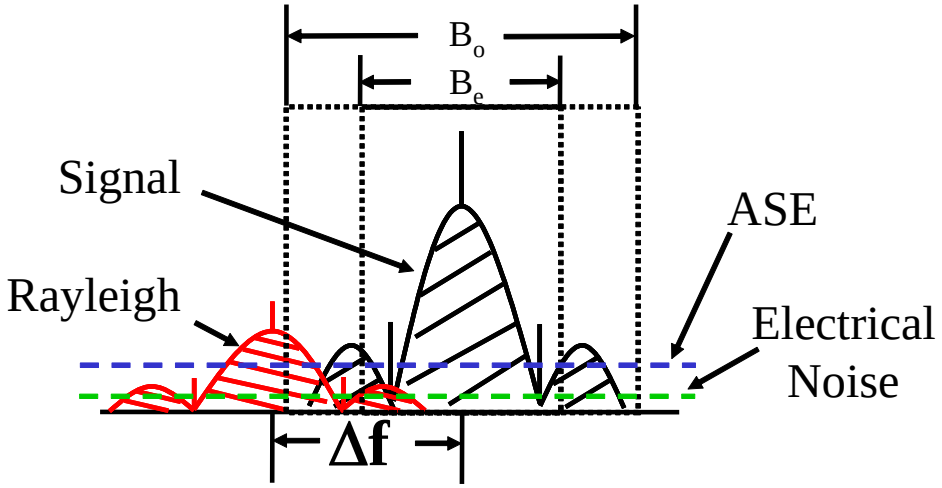

Fig. 2.2. Frequency domain illustration of the detection process of the W-E signal from Fig. 2.1. RB caused by the E-W channel is colored while ASE and electrical noise are white. The detected signal lies centered within the electrical bandwidth, B_e, and the optical bandwidth, B_o.

associated with RB, ASE and electrical noise must be calculated along with the signal distortions associated with optical and electrical filtering.

The mathematical formalism describing IM-DD link performance corrupted by RB, ASE and electrical noise at the detector will now be developed. In the theoretical treatment of RB and ASE noise, it is approximated that link performance is characterized by nearly-Gaussian noise statistics. In truth, such an approximation to the underlying noise statistics leads to slightly pessimistic results because the probability density functions (PDF) due to RB and ASE are not strictly Gaussian [5-8]. Nevertheless, these same studies show that the Gaussian approximation (GA) provides reasonable performance prediction provided that bit error rates are calculated using optimal decision thresholds thereby justifying its use. The motivation to use the GA is further supported due to the complex computation needed to evaluate link

performance based on *exact* statistics. As it has been shown, the enhanced accuracy gained by using exact noise statistics is often offset by the computational complexity [9, 10]. Therefore, the GA will be employed throughout this thesis and it will be demonstrated that this approximation agrees closely with experimental results.

The total power, p(t), detected by the PIN photodiode in Fig. 2.1 is given by

$$p(t) = \left| f_s(t) + f_{ASE}(t) + f_{RB}(t) \right|^2 . \tag{2.1}$$

where $f_s(t)$ is the optically filtered signal field and $f_{ase}(t)$ and $f_{rb}(t)$ are the optically filtered noise fields due to ASE and RB, respectively. The variance of the photocurrent is expressed as [11]

$$\sigma^2(t) = {R_D}^2 \int_{-\infty}^{\infty}\int_{-\infty}^{\infty} C_p(\tau,\tau')h(t-\tau)h(t-\tau')d\tau d\tau' . \tag{2.2}$$

where

$$C_p(\tau,\tau') = < p(\tau)p(\tau') > - < p(\tau) >< p(\tau') > . \tag{2.3}$$

R_D is the detector responsivity and h(t) represents the lowpass impulse response of the receiver circuitry. The first term in (2.3) represents the autocorrelation of the detected power. Because both ASE and RB are at least wide-sense stationary, uncorrelated, zero mean ccg random processes, the total variance is the sum of five possible terms [11]:

$${\sigma_{sig-ASE}}^2(t) = 2{R_D}^2 \Re\left\{ \int_{-\infty-\infty}^{+\infty+\infty} f_s(\tau)\, {f_s}^*(\tau') < {f_{ASE}}^*(\tau)\, f_{ASE}(\tau') > h(t-\tau)h(t-\tau')d\tau d\tau' \right\} \tag{2.4}$$

$${\sigma_{ASE-ASE}}^2 = M{R_D}^2 \Re\left\{ \int_{-\infty-\infty}^{+\infty+\infty} \left| < {f_{ASE}}^*(\tau)\, f_{ASE}(\tau') > \right|^2 h(t-\tau)h(t-\tau')d\tau d\tau' \right\} \tag{2.5}$$

$$\sigma_{sig-RB}{}^2(t) = 2R_D{}^2\Re\left\{\int_{-\infty-\infty}^{+\infty+\infty} f_s(\tau) f_s{}^*(\tau') < f_{RB}{}^*(\tau) f_{RB}(\tau') > h(t-\tau)h(t-\tau')d\tau d\tau'\right\} \quad (2.6)$$

$$\sigma_{RB-RB}{}^2 = R_D{}^2\Re\left\{\int_{-\infty-\infty}^{+\infty+\infty}\int |< f_{RB}{}^*(\tau) f_{RB}(\tau') >|^2 \; h(t-\tau)h(t-\tau')d\tau d\tau'\right\} \quad (2.7)$$

$$\sigma_{ASE-RB}{}^2 = 2R_D{}^2\Re\left\{\int_{-\infty-\infty}^{+\infty+\infty}\int < f_{ASE}{}^*(\tau) f_{ASE}(\tau') >< f_{RB}{}^*(\tau) f_{RB}(\tau') > h(t-\tau)h(t-\tau')d\tau d\tau'\right\} \quad (2.8)$$

where the factor M in (2.5) is the number of polarization modes present at the detector. If there is no polarizer before the detector, M = 2. In general, $f_s(t)$ represents the optically filtered signal field and h(t) is the lowpass impulse response of the receiver electronics. The terms $<f_{ase}{}^*(\tau)f_{ase}(\tau')>$ and $<f_{rb}{}^*(\tau)f_{rb}(\tau')>$ represent the autocorrelation functions (ACF) of the optically filtered ASE and RB noise field, respectively and is defined as

$$\langle f(t) f(t+\tau)\rangle = \int_{-\infty}^{+\infty} f(t) f(t+\tau) d\tau \,. \quad (2.9)$$

As can be seen in (2.4-2.8), it is the functional difference of the noise ACFs which distinguishes ASE from RB. Because ASE is a white noise process (i.e. has a flat spectral density), ACF_{ASE} is *delta-correlated* in the frequency domain. RB, on the other hand, has an ACF which depends on the spectral properties of the modulation format which generates the RB noise field.

Under the GA, the total noise corrupting the channel is given by

$$\sigma_{tot}^2(t) = \sigma_{sig-ASE}^2(t) + \sigma_{ASE-ASE}^2 + \sigma_{sig-RB}^2(t) + \sigma_{RB-RB}^2 + \sigma_{ASE-RB}^2 + \sigma_{elec}^2 \,. \quad (2.10)$$

where the photocurrent variance due to receiver electrical noise is

$$\sigma_{elec}^2 = R_D^2 NEP^2 B_e \,. \quad (2.11)$$

Here, NEP is the noise equivalent power and refers to the intrinsic noise spectral density of the receiver and is quoted in units of W/√Hz. This noise term accounts for electrical noise processes such as thermal noise and shot noise.

2.2 Analytic Noise Model: Gaussian Pulse and Filter Shapes

2.2.1 Analytic Noise Variance

It is possible to obtain closed-form solutions to (2.4-2.8) using a set of Gaussian approximations for the pulse and filter shapes in the link described in Fig. 2.1. This method was originally suggested by Winzer for the analysis of DRB in RA [12] and is now applied to RB in bidirectional links. The following approximations are used for the pulse shapes and filter shapes:

$$e_{sig}(t) = \sqrt{P_1} e^{-2\pi B_s^2 t^2} \xrightarrow{FT} S(f) = \frac{\sqrt{P_1}}{\sqrt{2}B_s} e^{-\frac{\pi f^2}{2B_s^2}}. \quad (2.12a)$$

$$n_{ASE}(t) = \sqrt{N_{ASE}}\delta(t) \xrightarrow{FT} N_{ASE}(f) = \sqrt{N_{ASE}}. \quad (2.12b)$$

$$n_{RB}(t) = \sqrt{2B_s P_{RB}} e^{-2\pi B_s^2 t^2} e^{i2\pi\Delta f t} \xrightarrow{FT} N_{RB}(f) = \sqrt{\frac{P_{RB}}{B_s}} e^{-\frac{\pi (f-\Delta f)^2}{2B_s^2}}. \quad (2.12c)$$

$$b(t) = \sqrt{2}B_o e^{-2\pi B_o^2 t^2} \xrightarrow{FT} B(f) = e^{-\frac{\pi f^2}{2B_o^2}}. \quad (2.12d)$$

$$h(t) = 2\sqrt{2}B_e e^{-8\pi B_e^2 t^2} \xrightarrow{FT} H(f) = e^{-\frac{\pi f^2}{8B_e^2}}. \quad (2.12e)$$

Here, P_1 is the peak power of a transmitted mark, N_{ASE} is the ASE power spectral density in a *single* polarization mode, P_{RB} is the *total* Rayleigh backscattered power,

b(t) is the optical filter impulse response, and B_s, B_o, B_e are the equivalent bandwidths of the signal spectrum, optical filter, and electrical filter, respectively. Furthermore, $f_s(t) = e_{sig}(t) \times b(t)$, $f_{ASE}(t) = n_{ASE}(t) \times b(t)$ and $f_{RB}(t) = n_{RB}(t) \times b(t)$ where × denotes convolution. It should be noted that the above functions represent the *field* of the optical light, not the intensity. The conversion to intensity is the magnitude squared of the field. Performing the convolution of the signal pulse with the optical filter gives signal optically filtered signal field:

$$f_s(t) = \frac{\sqrt{P_1}}{\sqrt{1+\frac{B_s^2}{B_o^2}}} \exp\left[-\frac{\pi B_s^2 t^2}{1+\frac{B_s^2}{B_o^2}} \right]. \tag{2.13}$$

assuming that the optical filter and the signal have perfectly aligned center frequencies.

It is important to point out that the filters given by (12-d) and (12-e) are defined by there *noise equivalent bandwidths* (NEB) and not their 3 dB bandwidths. It can be shown that the NEB bandwidth (B_{NEB}) of a Gaussian filter is exactly the same as that of an ideal, rectangular shaped filter. Thus, the total energy within the optical Gaussian filter is B_o and the total energy within the electrical filter is $2B_e$. The corresponding 3 dB bandwidth for a first order Gaussian filter evaluates to $0.94*B_{NEB}$.

2.2.1.1 Calculation of ASE Variances

The calculation of (2.4) is demonstrated by Winzer in [12]. For ASE, the constant power spectral density leads to an autocorrelation function dependent only on the optical filter bandwidth.

$$< f_{ASE}^{*}(\tau) f_{ASE}(\tau') >= N_{ASE} B_o e^{-\pi B_o^2 (\tau-\tau')^2} . \quad (2.14)$$

Plugging (2.14) into (2.4) and setting t = 0, we arrive at (6) in [12],

$$\sigma^2_{sig-ASE} = \frac{4R_D^2 N_{ASE} P_1 B_e}{\sqrt{1+\frac{B_s^2}{B_o^2}+\frac{B_s^2}{4B_e^2}}\sqrt{1+\frac{2B_s^2}{B_o^2}+\frac{4B_e^2}{B_o^2}\left(1+\frac{B_s^2}{B_o^2}\right)}} . \quad (2.15)$$

Plugging (2.14) into (2.5) and setting t = 0, the ASE-ASE beat noise is found to be

$$\sigma^2_{ASE-ASE} = \frac{2\sqrt{2} R_D^2 N_{ASE}^2 B_e B_o}{\sqrt{1+\frac{2B_e^2}{B_o^2}}} \quad (2.16)$$

where it is assumed that no polarizer is present at the detector (i.e. M = 2).

2.2.1.2 Calculation of RB Variance

To understand the effect of channel separation and RB in IB networks, use is made of the frequency shifting property of Fourier transforms [13]

$$x(t)e^{i2\pi\Delta f t} \xrightarrow{FT} X(f-\Delta f) . \quad (2.17)$$

where Δf is the frequency difference between the center frequency of the signal and optical filter and the center frequency of the interfering Rayleigh channel (see Fig. 2.2). The convolution of the shifted RB spectrum with the optical filter ($n_{RB}(t)*b(t)$) is

$$f_{RB}(t) = \frac{\sqrt{2B_s P_{RB}}}{\sqrt{1+\frac{B_s^2}{B_o^2}}} \exp\left[-\frac{2\pi B_s^2 t^2}{1+\frac{B_s^2}{B_o^2}}\right] \exp\left[-\frac{\pi\Delta f^2}{2B_o\left(1+\frac{B_s^2}{B_o^2}\right)}\right] \exp\left[\frac{i2\pi\Delta f t}{1+\frac{B_s^2}{B_o^2}}\right] . \quad (2.18)$$

Calculation of the autocorrelation of $f_{RB}(t)$ yields

$$< f_{RB}^{*}(\tau) f_{RB}(\tau') >= \frac{P_{RB}}{\sqrt{1+\frac{B_s^2}{B_o^2}}} \exp\left[-\frac{\pi B_s^2 (\tau-\tau')^2}{1+\frac{B_s^2}{B_o^2}} \right] \exp\left[-\frac{\pi \Delta f^2}{B_o\left(1+\frac{B_s^2}{B_o^2}\right)} \right] \exp\left[\frac{i2\pi\Delta f(\tau-\tau')}{1+\frac{B_s^2}{B_o^2}} \right]. \quad (2.19)$$

Plugging (2.19) into (2.6) and setting t = 0, the expression for the signal-RB beat noise variance as a function of filter bandwidths and frequency offset is

$$\sigma_{sig-RB}^2 = \frac{2\eta_{pol} R_D^2 P_{RB} P_1}{\sqrt{1+\frac{B_s^2}{B_o^2}} \sqrt{1+\frac{2B_s^2}{B_o^2}+\frac{B_s^2}{2B_e^2}} \sqrt{1+\frac{B_s^2}{B_o^2}+\frac{B_s^2}{4B_e^2}}} \exp\left(-\frac{\pi\Delta f^2 \left(4+\frac{4B_s^2}{B_o^2}+\frac{2B_s^2}{B_e^2}+\frac{B_o^2}{B_e^2}\right)}{2B_o^2\left(1+\frac{B_s^2}{B_o^2}\right)\left(2+\frac{2B_s^2}{B_o^2}+\frac{B_s^2}{B_e^2}\right)} \right) \quad (2.20)$$

where the term η_{pol} represents the fraction of RB light which is co-polarized with the signal. For a common low birefringence fiber, the RB light will have a degree of polarization (DOP) which is approximately 33% of the original launched light [14]. Therefore, if the original light is nearly 100% polarized, as is often the case, the RB will have a DOP of 33%. A DOP of 33% implies that 2/3 of the light remains in the original polarization while 1/3 of the light scatters into the orthogonal polarization. Under these condition, η_{pol} = {1/3, 2/3}. When η_{pol} = 2/3 the signal and Rayleigh will be optimally aligned and the greatest penalty from coherent Rayleigh beating will be incurred. If η_{pol} is set to 1 and Δf is set to 0, (2.19) and (2.20) collapse to become equations (5) and (7) in [12].

By plugging (2.19) into (2.7) and setting t = 0, the expression for the RB-RB beat noise becomes

$$\sigma_{RB-RB}^2 = \frac{2R_D^2 P_{RB}^2}{\sqrt{1+\frac{B_s^2}{B_o^2}} \sqrt{1+\frac{B_s^2}{B_o^2}+\frac{B_s^2}{2B_e^2}}} \exp\left(-\frac{2\pi\Delta f^2}{B_o^2\left(1+\frac{B_s^2}{B_o^2}\right)} \right). \quad (2.21)$$

Lastly, plugging (2.14) and (2.19) into (2.8) and setting t = 0 yields

$$\sigma_{ASE-RB}^2 = \frac{4R_D^2 N_{ASE} P_{RB} B_e}{\sqrt{1+\frac{2B_s^2}{B_o^2}+\frac{4B_e^2}{B_o^2}\left(1+\frac{B_s^2}{B_o^2}\right)}} \exp\left(-\frac{2\pi\Delta f^2\left(1+\frac{2B_e^2}{B_o^2}\right)}{B_o^2\left(1+\frac{2B_s^2}{B_o^2}+\frac{4B_e^2}{B_o^2}\left(1+\frac{B_s^2}{B_o^2}\right)\right)}\right). \quad (2.22)$$

The key information to be gleaned from (2.20-2.22) is that the effect of RB noise can be significantly mitigated in the receiver when the channel offset is increased. This reduction in noise trends as a decaying exponential whose decay constant is proportional to the square of the frequency offset. Hence, RB becomes negligibly small for large channel separations. Unfortunately, only partial insight can be gained from the impact of filtering on the reduction of the noise due to the complicated inter-relationship between Gaussian pulse width and optical and electrical filter bandwidth. Nonetheless, narrower filter bandwidths translate to smaller RB noise variances as will become obvious later. The extent to which optimal filtering can suppress RB noise will be the primary subject of Chapter 3.

2.2.2 Quantifying Link Performance: BER and Q-factor

The figure of merit which most reliably characterizes communication systems is bit error rate (BER). It is well known that a communications system degraded by Gaussian noise has a BER given by

$$BER = \frac{1}{2} erfc\left(\frac{Q}{\sqrt{2}}\right). \quad (2.23)$$

where the Q-factor is

$$Q = \frac{\mu_{1-} - \mu_0}{\sigma_1 + \sigma_0}. \quad (2.24)$$

Here, μ_1 and μ_0 are the mark and space photocurrents at the sampling instant, respectively, and σ_1 and σ_0 are the mark and space noise variance, respectively. Therefore, knowledge of the signal waveform and the noise variance of marks and spaces determines the BER of the transmission in Gaussian noise dominated communication systems. For the analytic model, BER is conveniently calculated using (2.11), (2.12), (2.15), (2.16) and (2.20-2.22). To avoid a more detailed and tedious analysis, the method used to relate the parameters of the analytic model to experimentally measured quantities is saved for Appendix III.

2.2.3 Limitations of the Analytic Model

Unfortunately, the analytic model has two critical limitations. First, the analytic model assumes that all pulse and filter shapes can be approximated as having 1^{st} order Gaussian shapes. Although this approximation allows for calculation of closed-form equations for the noise variances, realistic modulation formats can have distinctly non-Gaussian PSDs (as illustrated in Appendix II). Secondly, while the analytic model successfully describes the impact of filtering on noise mitigation, it does not accurately account for the deleterious impact of filter induced inter-symbol interference (ISI). Although attempts are made to account for the effect of ISI on the analytic model (as described in Appendix III), an alternative approach is warranted to produce more accurate results.

2.3 Numerical Noise Model: Exact PSD and Filtering Effects

The limitations imposed by the analytic model are eliminated with the implementation of a more powerful numerical model. In this section, a full numerical model which calculates ASE and RB noise variances is detailed which solves (2.4-2.8) using exact PSD and filtering effects. The numerical noise model is adapted from previous models used to study the impact of ASE on conventional optical links [15-18]. Instead, however, the approach is generalized to include RB impairments. Just as with the analytic model, the numerical model solves (2.4-2.8) and calculates Q-factor and BER. In this case, the double integrals of the noise variance equations are solved by numerical methods using MATLAB® (The MathWorks). Since closed-form solutions are not necessary, realistic filter and pulse shapes allow for a more accurate BER calculation.

Some of the most important differences between the analytic and numerical model are highlighted in the next section. Further details regarding the numerical model will be described in Chapter 3.

2.3.1 Exact PSD and ACF

The first improvement afforded by numerical calculation of (2.4-2.8) is that exact RB PSD can be implemented. Because RB noise has a PSD proportional to the generating field [19], the frequency content of the RB beat noise is highly dependent on modulation format [12, 20-22]. In (2.4-2.8), the frequency dependence of the beat noise characteristics is described by the ACF term, $\langle f_{ase/rb}^{*}(\tau) f_{ase/rb}(\tau') \rangle$. Since RB and

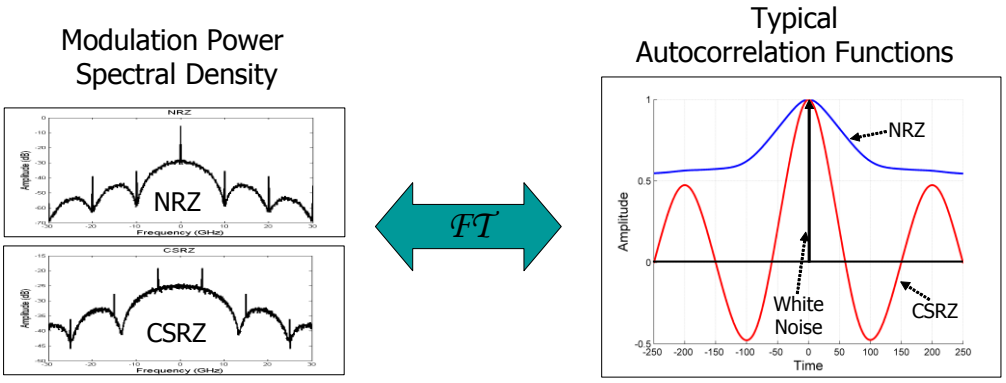

Fig. 2.3. Illustration showing the Fourier Transform relationship between the modulation PSD and the respective ACF. Figures are generated using the numerical model code.

ASE are both (at least) WSS[2], the PSD is Fourier Transform related to the ACF via the Wiener-Khinchin theorem [23]. In mathematical form

$$R(\tau) = \int_{-\infty}^{\infty} S(f) e^{-j2\pi f\tau} df \ . \tag{2.25}$$

where R(τ) is the ACF of the noise process having the PSD S(f). Using the fast Fourier Transform (fft) and inverse fast Fourier Transform (ifft) functions in MATLAB, converting between of R(τ) and S(f) is straightforward. Examples of the ACF calculation using the MATLAB code are shown in Fig. 2.3 for NRZ and CSRZ modulation formats.

2.3.2 Filter-induced ISI and BER Calculation

The ability to simulate realistic filter induced ISI is the other main advantage of the numerical model. For this reason, the ever-present tradeoff between noise cancellation and filter-induced distortions can be accurately modeled. This advantage is particularly important because BER performance tends to be dominated by worst

[2] For more details on the underlying statistics of RB, see Appendix I.

case patterning effects [24]. Physically, bit patterns like isolated marks have the highest frequency content and are thus more susceptible to LPF distortions resulting in a higher probability of bit errors.

To study the impact of filtering, a 4th order Bessel filters is used in the model. Bessel-type LPFs are the electrical filter of choice in telecom systems owing to their linear group delay in the pass band. This linear phase response results in minimal ripple in the filtered pulses. The transfer function of the 4th order Bessel filter used in this model is given by [25]

$$H(s) = \frac{105}{s^4 + 10s^3 + 45s^2 + 105s + 105} \tag{2.26}$$

where s=jω. The 1st order Gaussian optical filter described by (2.12d) is used to simulate the demux filter shape [26].

Patterning effects due to the transmission of random bit sequences are incorporated into the model using pseudo-random bit sequences (PRBS). The use of PRBS patterns is a common practice in fiber telecom research and has been shown to accurately model pattern randomness for moderate numbers of bits [16, 18]. In this work, pattern dependent ISI is simulated using PRBS patterns of length 2^7-1. Given the temporal field amplitude of a PRBS modulated signal, esig(t), the optically and electrically filtered photocurrent is

$$s(t) = R_D \left| G \cdot e_{sig}(t) \otimes b(t) \right|^2 \otimes h(t). \tag{2.27}$$

The calculation of BER is modified in the numerical model using the waveform at the decision circuit, s(t), is known. In this case, BER is calculated on a

bit by bit basis and the total BER is averaged over all bits. The effect of filtering will be accurately modeled because pathological bit sequences will tend to dominate BER performance. The total BER for the entire sequence is found by substituting (2.10) and (2.27) into the relation

$$BER(t_s, s_{th}) = \frac{1}{N}\left\{\sum_{k_0}\frac{1}{2}erfc\left(\frac{\left(\frac{s_{th} - s(t_s + k_0 T)}{\sigma(t_s + k_0 T)}\right)}{\sqrt{2}}\right) + \sum_{k_1}\frac{1}{2}erfc\left(\frac{\left(\frac{s(t_s + k_1 T) - s_{th}}{\sigma(t_s + k_1 T)}\right)}{\sqrt{2}}\right)\right\}. \quad (2.28)$$

Here, t_s is the sampling instant, s_{th} is the decision threshold, N is the number of bits in the sequence and k_0 and k_1 are indexes used to distinguish between transmitted marks and transmitted spaces. The first summation in (2.28) represents the probability of receiving a mark given that a space was sent (i.e. P(0|1)) while the second summation represents the probability of receiving a space given that a mark was sent (i.e. P(1|0)). The scaling term in the front of (2.28) averages the total BER over all bits (in this case, N is 127 bits).

2.4 10 Gb/s Experiments: NRZ, RZ and DB

Rigorous experimental work was conducted in order to verify the accuracy of the two models. The following section describes the experimental procedure for measuring the impact of RB on 10 Gb/s IM-DD systems. Three modulation formats are studied: NRZ, RZ and DB. The experimental and theoretical results verify the importance of RB in IB links and suggestions are made for noise penalty reduction.

2.4.1 Preliminary Results

2.4.1.1 NRZ, RZ and DB Transmitters

The first task was to construct two 10 Gb/s optical transmitters for NRZ, RZ and DB modulation. Details regarding the properties of these modulation formats can be found in Appendix II. After a rigorous evaluation of various optoelectronic component combinations from various manufacturers, appropriate driver-modulator combinations were determined for NRZ, RZ and DB. It was determined that excellent NRZ signals could be created with Picosecond Pulse Labs drivers (PSPL 5865) and JDSU 10 Gb/s Mach-Zehnder modulators (MZM). RZ modulation (50% duty cycle) was created by cascading the NRZ transmitter with a JDSU pulse carving modulator driven with a 10 GHz clock. DB was a considerably more challenging format to create due its enhanced complexity and need for twice the driver voltage [27]. Ultimately, high performance DB signals were achieved with a specific combination of Triquint drivers (TGA4954-SL) and Avanex Duobinary-class MZMs (Powebit^{TM} F-10-D). Owing to their applicability in many current and future projects at UCSD, these 10 Gb/s NRZ and DB transmitters were conveniently packaged within mechanically stable, portable, rack mountable boxes with dedicated power supplies and heat sinks. The NRZ box, in particular, was used throughout the experimental work of Chapters 4 and 5. Eye diagrams and modulation spectrums are shown in Fig. 2.4.

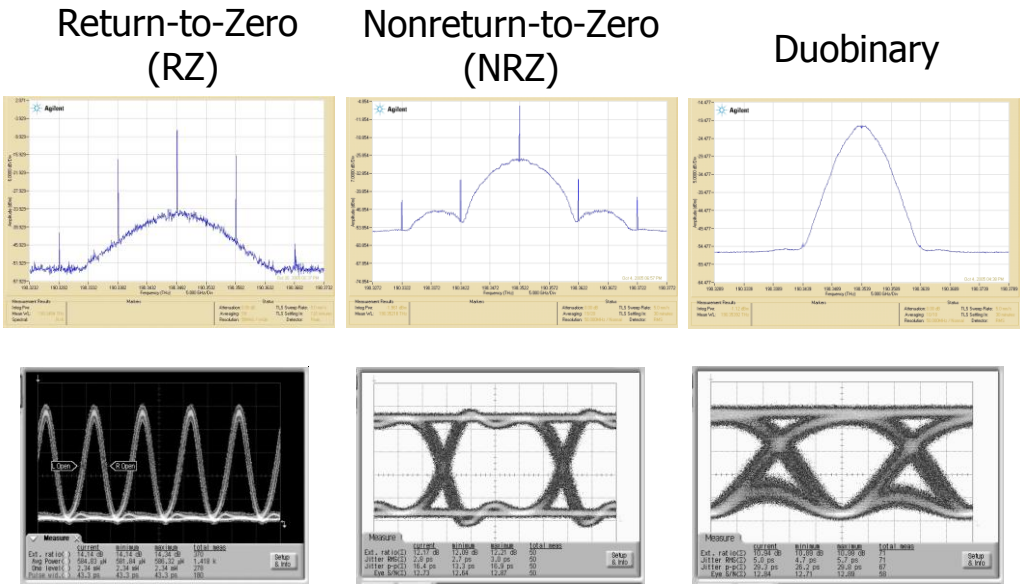

Fig. 2.4. Experimental modulation spectra and eye diagrams for 10 Gb/s RZ, NRZ and DB.

2.4.1.2 Rayleigh and Brillouin Scattering Regimes

With the newly constructed transmitters for NRZ, RZ and DB, it was now important to characterize the backscattered light coming from the fiber. In particular, it was important to characterize power limitations imposed by stimulated Brillouin scattering (SBS) in the fiber. SBS is a well-known nonlinear impairment in which limits the amount of launchable power into a fiber. Brillouin scattering is the inelastic scattering of photons by small density fluctuations in the transmission medium caused by interactions with acoustic phonons [28]. At low input powers, (spontaneous) Brillouin scattering is caused by thermal fluctuations in the fiber and is a relatively weak interaction which yields symmetrical back-reflected Stokes and anti-Stokes waves shifted in frequency by 10-12 GHz, depending on the fiber type. In most cases, spontaneous Brillouin scattering is considerably smaller than RB and can be neglected

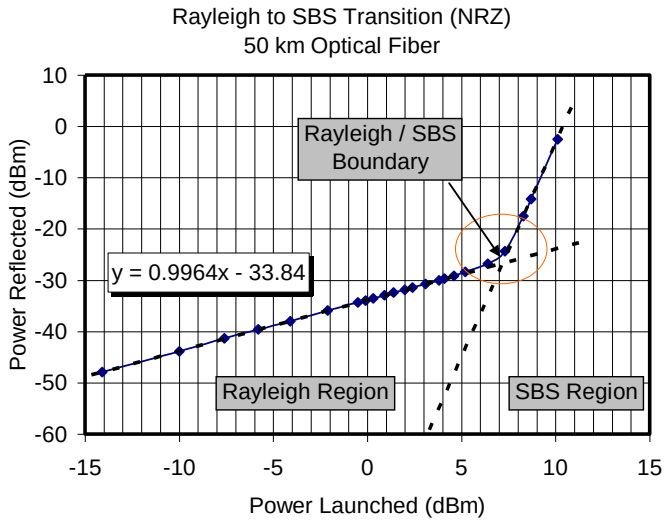

Fig. 2.5. Backreflected power versus launched power into single mode fiber. In the Rayleigh region, the reflected power increases dB for dB with launched power. At the onset of SBS, backreflected power begins to increase rapidly after the Rayleigh/SBS boundary.

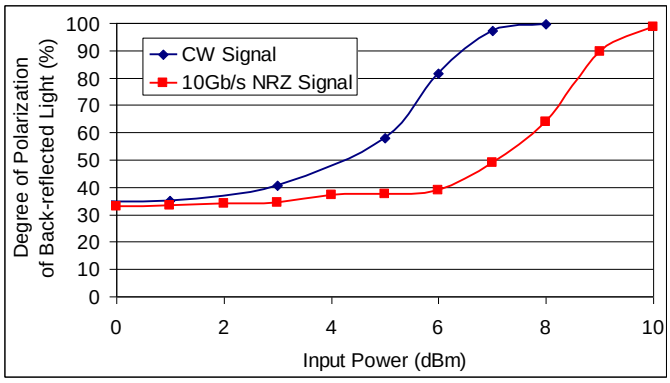

Fig. 2.6. Degree of polarization of the backreflected light versus input power. In the Rayleigh region the DOP is 33% [14]. As launch power increases, DOP increases towards 100% since SBS light is polarized [29].

[30, 31]. However, as launch powers increase, the strong electric field of the incident light causes periodic refractive index fluctuations in the fiber through the process of electrostriction. This induced periodicity serves as a moving acoustical grating which backscatters frequency-shifted light by the process of Bragg diffraction. Above the

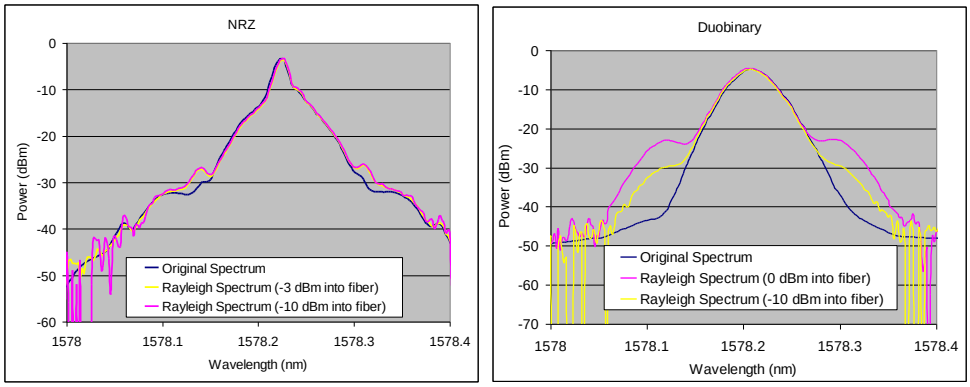

Fig. 2.7. RB spectrums for NRZ and DB. Stokes shifts of +/-11 GHz visible due to spontaneous Brillouin scattering. RB PSD is proportional to the launched PSD.

Brillouin threshold, the efficiency of the stimulated Brillouin process grows rapidly resulting in a majority of the backscattered light to be caused by SBS. In bidirectional links, SBS limits the amount of transmitted power through the fiber and causes large asymmetries in channel spacing allocation due to the Stokes-wave frequency shift [31, 32]. For the theoretical work in this thesis, linear channels are assumed which ensures that that the PSD of backscattered light is proportional to that of the launch field.

To maintain the validity of the theoretical models, experimental powers must therefore be kept smaller than the SBS threshold. Under these conditions, backscattering of light is primarily due to by Rayleigh scattering processes and the backscattered PSD will be proportional to the launched PSD. The dependence of backscattered signal strength on launch power is illustrated in Fig. 2.5. As long as the launched light is kept below approximately +7 dBm, reflected power is linearly proportional to launch power thus guaranteeing that RB is the dominant backscattering process.

It should be clarified that the exact Brillouin threshold is dependent on modulation format, laser linewidth and fiber-type. It is well known that the onset of SBS can be pushed towards higher powers with techniques such as frequency dithering, linewidth broadening, carrier suppression, applied strain, line coding and fiber waveguide engineering [33-37]. In the setup used to generate Fig. 2.5, NRZ modulation was used which, when compared to RZ and DB, yields conservative SBS thresholds because of the much stronger carrier tone. By contrast, DB has been shown to delay onset of SBS by as much as 12.6 dB compared to NRZ at 10 Gb/s [38]. Nevertheless, the experiments in this work never exceed launch powers of 0 dBm thereby guaranteeing that the backscattered light is caused almost entirely by Rayleigh scattering processes. The dominance of RB below 0 dBm is further demonstrated in Fig. 2.6 since the degree of polarization (DOP) of the reflected light is 33% for launched powers less than the Brillouin threshold.

To verify that the PSD of RB is indeed proportional to the launch field, backreflected PSDs were measured for several input powers as shown in Fig. 2.7. It is shown that the backscattered spectrum changes very little as a function of launch power which is a characteristic of the Rayleigh process. Although Stokes and anti-Stokes sidebands are clearly visible, these contributions are negligibly small since Fig. 2.7 plotted on a *logarithmic* scale. Furthermore, the backreflected spectra are symmetrical verifying the SBS can be ignored at launch powers below 0 dBm.

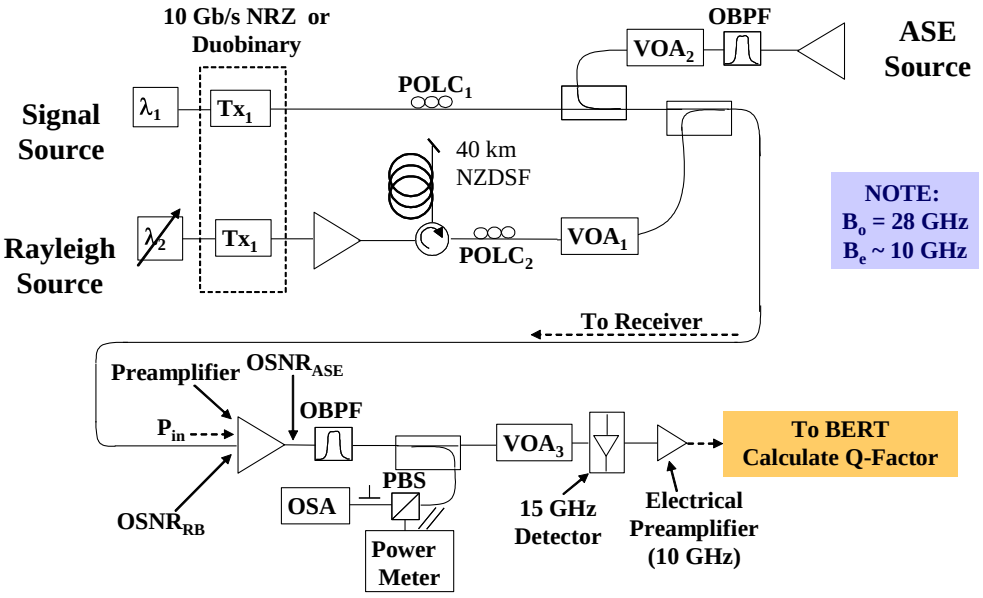

Fig. 2.8. Experimental setup. Polarization Controller—POLC. Variable optical attenuator—VOA. Polarization beam splitter—PBS. Bit error rate tester—BERT. Optical spectrum analyzer—OSA.

2.4.2 Noise Limited Results and Theoretical Comparison

2.4.2.1 Experimental Setup

The experimental setup used to measure the impact of RB in IB links is shown in Fig. 2.8. The setup constructed to validate the generalized noise model makes use of three independently controlled arms allowing for careful manipulation of the Signal, RB and ASE characteristics. By varying λ_2, VOA_1, VOA_2, $POLC_1$ and $POLC_2$ it was possible to measure the Q-factor of the received signal as a function of Δf, optical signal to noise ratio due to RB ($OSNR_{RB}$), optical signal to noise ratio due to ASE ($OSNR_{ASE}$) and polarization alignment. Q-factor was measured using the decision threshold technique in [39]. By definition, $OSNR_{RB}$ was measured

immediately before the optical pre-amp and represents the ratio of signal power divided by RB power (neglecting power contribution from ASE). Additional ASE was introduced by the booster in the Rayleigh arm of the experiment but was neglected since the OSNR prior to the circulator exceeded 40 dB (within a 0.1 nm bandwidth). $OSNR_{ASE}$ was measured immediately after the preamplifier in the absence of RB noise (Tx_1 was turned off). Launched power levels into the fiber never exceeded 0 dBm in order to avoid Brillouin scattering and to prevent unwanted nonlinear effects as will be demonstrated later. The influence of the preamplifier performance was carefully factored out: noise figure variability with respect to the input power (P_{in}) was eliminated by maintaining a constant input power of -24 dBm, unless otherwise noted. The minimum preamplifier input power resulted in an output $OSNR_{ASE}$ of 30 dB thus minimizing the impact of preamplifier excess noise. The power into the detector was held constant at -7 dBm using VOA_3 which helped to guarantee that optical noise (i.e. ASE and RB) dominated signaling performance compared to electrical receiver noise (electrical noise sensitivity <-17 dBm). The receiver bandwidth was 10 GHz and was limited by the electrical pre-amplifier.

2.4.2.2 ASE Dominated Performance

The performance of NRZ, RZ and DB under ASE dominated conditions is shown in Fig. 2.9. Using the fitting techniques described in Appendix III, Fig. 2.9 illustrates that both the analytic and numerical models both perform extremely well in comparison to experiment. Indeed, theoretical and experimental results show agreement typically better than 0.5 dB! Considering the numerous sources of possible

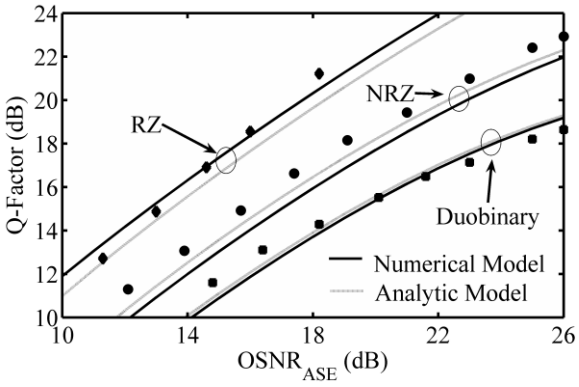

Fig. 2.9. Comparison of theory and experiment for ASE dominated performance.

error (non-Gaussian filter roll-off, nonlinear filter group delay, non-Gaussian shaped pulses, non-ideal electrical amplifier characteristics, measurement error, etc…), such agreement demonstrates the validity of the underlying assumptions for white noise processes like ASE. Although the analytic and numerical models solve (2.4-2.8) using distinct approaches, it is clear that both models yield similar predictions for performance of ASE dominated links.

2.4.2.3 ASE/RB Hybrid Performance ($\Delta f = 0$)

Having justified the merits of the theoretical approach for the analytic and numerical models for ASE, it is now possible to incorporate RB. The first task is to determine how ASE and RB combine as performance transitions from ASE dominated to RB dominated regimes. The theoretical and experimental results demonstrating this

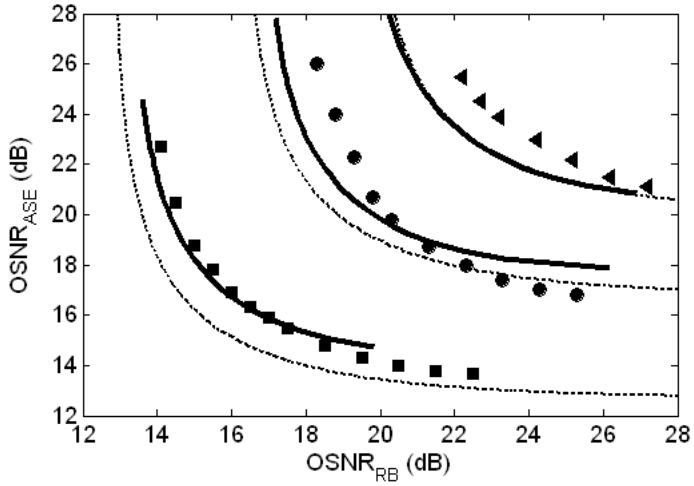

Fig. 2.10. Contour plots of constant Q = 6 for combination of ASE and coherent RB. Dashed line—analytic model. Solid line—numerical model. Marks—experimentally measured data.

transition for perfectly overlapped (coherent) RB is shown in Fig. 2.10. By inspection of (2.10) and (2.24) it is apparent that the transition between the ASE and RB noise regimes is characterized by a 1/x-type relationship in the Q-factor performance. When RB is small and ASE is high, Q-factor (and hence BER) is asymptotic as is illustrated in Fig. 2.10 by the horizontally asymptotic region. When RB is large and ASE is small, Q-factor performance transitions towards a vertically asymptotic behavior as indicated in Fig. 2.10. Between these two regimes, a smooth 1/x transition exists in which both ASE and RB noises have similar magnitudes and neither can be neglected.

An important question arises: when is it acceptable to assume that only a single noise process dominates performance? Based on Fig. 2.10, a convenient rule of thumb can be ascertained: *if the absolute difference in $OSNR_{ASE}$ and $OSNR_{RB}$ is greater than approximately 8 dB, then link performance will be dominated by the largest noise term*. In other words,

$$OSNR_{RB} \geq OSNR_{ASE} + 8dB \Rightarrow \text{ASE Dominated} \quad (2.29)$$

$$OSNR_{ASE} \geq OSNR_{RB} + 8dB \Rightarrow \text{RB Dominated.} \quad (2.30)$$

This "8 dB rule" carries the caveat that it is only true at 10 Gb/s. By definition, $OSNR_{ASE}$ sensitivity is a data rate *dependent* quantity because it characterizes the noise power spectral density of ASE over a specific bandwidth (as opposed to just the noise power). The implication is that the required $OSNR_{ASE}$ to achieve Q = 6 (i.e. BER $\approx 10^{-9}$) scales with data rate. As an example, Fig. 2.9 shows that NRZ achieves Q = 6 (i.e. 15.5 dB) for $OSNR_{ASE}$ = 16 dB. If all else is equal, the required $OSNR_{ASE}$ for NRZ at 40 Gb/s would be 22 dB (16 dB + 10log(40e9/10e9)). By contrast, RB sensitivity is by definition data rate independent and thus does not require data rate scaling [11]. A more general, data rate independent rule of thumb can be written as

$$OSNR_{RB} \geq OSNR_{ASE} + 8dB - 10\log(R/10^{10}) \Rightarrow \text{ASE Dominated} \quad (2.31)$$

$$OSNR_{ASE} \geq OSNR_{RB} + 8dB + 10\log(R/10^{10}) \Rightarrow \text{RB Dominated.} \quad (2.32)$$

From these OSNR definition considerations, it is possible to predict whether a link will be limited by ASE, RB or both ASE and RB, regardless of data rate.

2.4.2.4 RB Dominated Performance ($\Delta f \neq 0$)

Fig. 2.11 shows the Q-factor performance of 10 Gb/s non-return to zero (NRZ), return to zero (RZ) and Duobinary (DB) as a function of $OSNR_{RB}$ for coherent RB crosstalk (Δf = 0) and incoherent RB crosstalk (Δf = 10 GHz). It is clear from these results that both models accurately predict coherent RB limited performance within 1 dB accuracy. When the RB channel offset equals the data rate (10 GHz), the

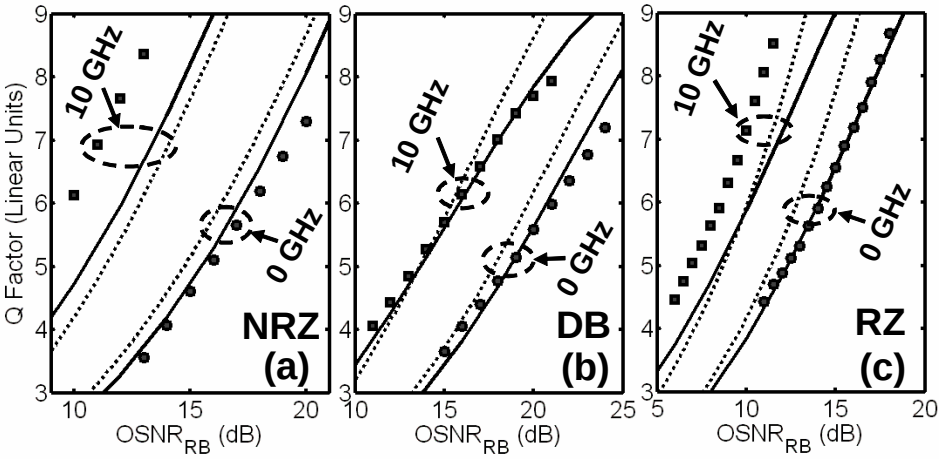

Fig. 2.11. Results showing copolarized RB impact on Q-factor for Δf = 0 and Δf = 10 GHz for (a) NRZ (b) DB (c) RZ. Markers—measured points. Solid curve—exact PSD solution, dashed—approximate PSD solution.

accuracy of both models degraded in terms of absolute Q performance. For NRZ and RZ formats, the numerical model exhibited maximal 2 dB error and the analytic model had maximal 3 dB prediction error compared to the experimental data. Interestingly, the predicted performance of DB impaired by incoherent RB crosstalk was significantly more accurate with excellent agreement (< 1 dB error) for both models.

The required $OSNR_{RB}$ to maintain Q = 6 as a function of increasing Δf is plotted in Fig. 2.12. The curves are normalized to the worst case sensitivity (Δf = 0, co-polarized signal and RB). The numerical model was superior for predicting the sensitivity improvement for all modulation formats and all frequency offsets. DB, for example, had better than 1 dB agreement for all polarizations and offsets up to 15 GHz. Prediction of NRZ and RZ performance also had better than 1 dB discrepancy, except between 7.5-10 GHz. The largest error around 7.5 GHz (3 dB for NRZ, 2 dB

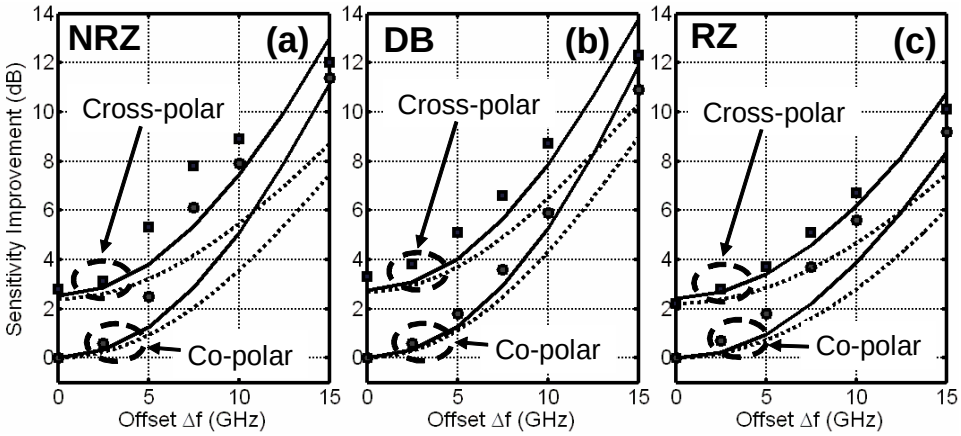

Fig. 2.12. Theoretical and experimental results showing enhanced RB sensitivity for larger offset, Δf, for (a) NRZ (b) DB (c) RZ. Markers—measured points. Solid curve—numerical solution, dashed—analytic solution.

for RZ) is attributed to uncertainties in the exact filter rolloff. When Δf approaches the data rate, performance becomes increasingly sensitive to the exact filter response. Since NRZ and RZ have strong DC components, small errors in the rolloff estimation results in large swings in sig-RB beating for Δf near the bit rate. This argument is supported by the fact that NRZ, with the largest DC component, has the most significant prediction error. Above 10 GHz, better agreement is achieved because RB-RB beating, which is homodyned to baseband, tends to limit performance. At 15 GHz spacing, typical agreement of 1 dB agreement is achieved. For NRZ, the numerical prediction accuracy using exact RB PSD outperforms the analytic model by better than 4 dB.

2.4.2.5 Incoherent RB and the Impact of Optical Filtering

When studying the results of section 2.4.2.4, it is interesting to note that RZ modulation has superior performance to NRZ and DB. These results are consistent

with previous work on coherent RB noise [20-22]. The explanation for the superiority of RZ over NRZ and DB stems from the fact that spectrally broader modulation formats generate higher frequency beat noise during square-law detection. This high frequency noise tends to be filtered by the finite bandwidth of the receiver electronics. On the other hand, narrower modulation formats like NRZ and DB generate comparatively lower bandwidth beat noise which passes unfettered to the decision circuit. Thus, spectrally broad modulation formats like RZ tend to tolerate significantly larger amounts of RB noise and are the prudent choice in optical links limited by coherent RB.

For the case of incoherent RB noise in IB links, however, a new design paradigm is expected because a great majority of incoherent RB noise can be rejected using properly designed optical filters (as depicted in Fig. 2.2). Intuitively, implementation of spectrally narrow modulation formats should lead to greater incoherent RB rejection for a given channel spacing because spectrally narrow formats tend to optimize for narrower optical filter bandwidths [40]. The experimental results were obtained with a 28 GHz optical filter. It has been shown, however, that optimal optical filtering of NRZ and DB is significantly narrower with optimal values varying from 14 GHz for NRZ to 7 GHz for DB [16, 40, 41].[3] To demonstrate the importance of optical filtering on incoherent RB mitigation, Fig. 2.13 plots the required channel spacing between IB channels for errorless performance using FEC versus the

[3] Optimal filter values are for ASE dominated links. At the time of this work, no rigorous study had been conducted to describe optimal optical filter design in the presence of incoherent RB noise. A detailed examination of the impact of incoherent RB noise on receiver design will be saved for Chapter 3.

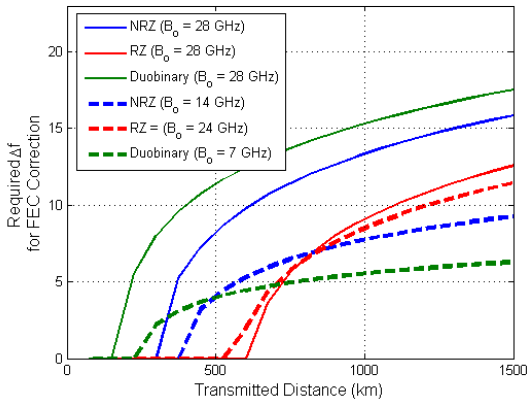

Fig. 2.13. Required channel spacing in an IB topology to achieve errorless signaling using FEC. Solid lines correspond to non-ideal demux bandwidths (28 GHz). Dashed lines correspond to "ideal" ASE optimized demux bandwidths. Beyond 700 km, DB has superior performance in terms of SE.

achievable distance. Recalling from Chapter 1, bidirectional links using NRZ are limited to about 400 km due to coherent RB noise. However, as channel spacing is increased, achievable distance is increased because incoherent RB can be successfully filtered in the optical and electrical domains. Furthermore, when format-tailored optical filters are implemented (as indicated by the dashed lines), huge improvements in RB sensitivity are gained because a significantly larger portion of incoherent RB is rejected. Hence, the inherent advantage of RZ in coherent RB dominated links can be overcome by DB and NRZ in incoherent RB dominated links if format-tailored filtering is used. In this case, the results of Fig. 2.13 show that IB link distances longer than about 700 km can achieve the highest RB immunity using spectrally narrow modulation formats such as DB. This new insight is of prime interest in the quest towards high spectral efficiency UDWDM systems.

2.4.3 Discussion: Analytic vs. Numerical Model

It has been shown that the accurate modeling of RB noise is critically dependent on modulation format and frequency offset. It is found that DB is well approximated by the analytic model because the PSD of DB is well approximated by a 1^{st} order Gaussian. However, NRZ and RZ have non-negligible carrier (> 50% for NRZ) and higher harmonic tones which cause the Gaussian PSD approximations to be unrealistic. Use of approximated PSD leads to an incorrect estimation of the frequency content of the *filtered* beat noise. For coherent RB, this effect is minimal since the majority of the beat noise falls within the optical and electrical filter bandwidths. However, the effect is exacerbated for incoherent RB since the filtering tends to reject large portions of the interchannel beat noise. Disparities between the exact and approximated PSD and/or filter rolloff result in large deviations between predicted and actual incoherent RB-limited performance.

Fig. 2.14 illustrates the importance of modeling incoherent RB using exact PSD. The total sig-RB beat noise is plotted for approximate (dotted) and exact (solid) PSD as a function of the frequency offset for NRZ (square) and DB (star), normalized with respect to the unfiltered worst case. Effectively, Fig. 2.14 plots the amount of sig-RB rejection afforded by the combination of frequency separation and optical filtering assuming a 10 GHz electrical bandwidth. Clear deviations exist between NRZ and DB modulation. For the 28 GHz optical filter, the approximated NRZ PSD underestimates the impact of frequency separation by 3 dB compared to the exact calculation. This corroborates well with the 4 dB experimental error in Fig. 2.12a.

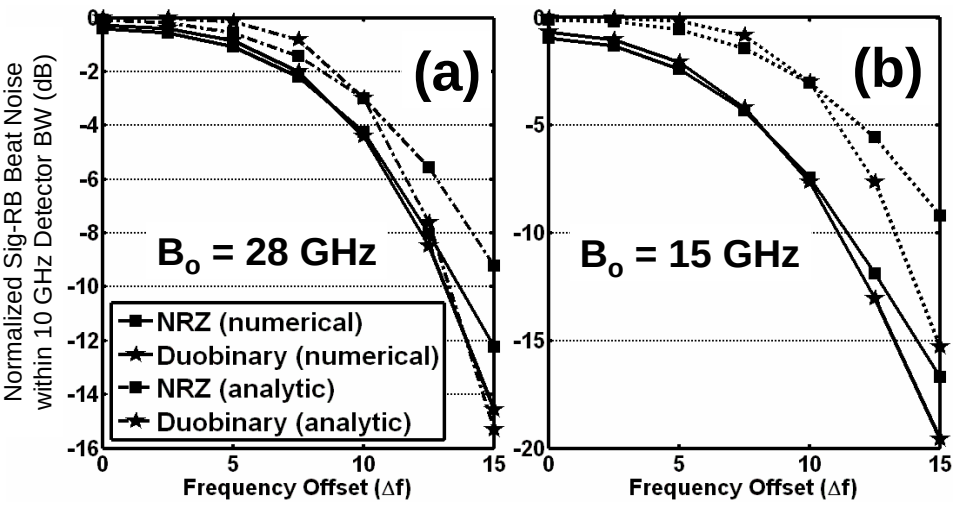

Fig. 2.14. Normalized Signal-RB beat noise within a 10 GHz detector bandwidth for exact and approximate PSDs. (a) B_o = 28 GHz, (b) B_o = 15 GHz. Discrepency between analytic and numerical models for DB is smaller and for NRZ.

The DB formatted channel, contrastingly, has less than 1 dB deviation. When the optical filter is roughly halved to 15 GHz (Fig. 2.14b), as might be necessitated in a high capacity bidirectional UDWDM system, the maximum error is increased to 8 dB and 4 dB for NRZ and DB, respectively. This large disagreement illustrates the importance of using exact PSDs when designing high capacity interleaved bidirectional networks impaired by incoherent RB noise.

In summary, the rigorous frequency characteristics of RB noise are required when calculating penalties in RB limited optical systems. These results demonstrate that while RB PSD approximations are adequate for coherent crosstalk, nothing short of the exact RB PSD can be used for the case of incoherent crosstalk, especially when narrow optical filtering is implemented to reject interchannel crosstalk. Although closed form solutions are preferred to calculate RB noise variance and is the preferred

approach to generating lookup network control algorithms, numerical modeling proves to be a considerably more accurate technique for high density bidirectional UDWDM links.

2.5 Conclusion

This chapter has been primarily concerned with the modeling and experimental measurement of coherent and incoherent RB noise in bidirectional optical links. Closed-form solutions for the generalized RB beat noise were derived using 1^{st} order Gaussian approximations and it was found that noise reduction via frequency offsetting scaled as a decaying exponential dependent on the offset squared (Δf^2). To incorporate the important effects of filter-induced ISI and exact RB PSD, a numerical model was developed. By comparing the theoretical and experimental results, several important conclusions have been made. First, it was demonstrated that the proper choice of modulation format in links degraded by RB noise depends on the frequency offset between interfering channels and the optical filter bandwidth. It was determined that IB links can achieve their highest spectral efficiencies if spectrally narrow modulation formats are implemented in conjunction with format tailored optical filtering.

The second major contribution of this chapter is that the numerical model must be used when calculating impact of incoherent RB in UDWDM IB links. Although the analytic model performs well for coherent RB noise and DB modulation, its broad assumptions belie many important design subtleties necessary for optimal IB link design. Owing to the colored nature of RB noise, exact RB PSDs and filter-induced

ISI must be included when designing IB links. For this reason, the numerical model developed in this chapter will be utilized in Chapter 3 in order to design optimal receivers limited by RB noise.

ACKNOWLEDGEMENT

This chapter is, in part, a reprint of the material in "Performance of NRZ and duobinary modulation formats in Rayleigh and ASE-dominated dense optical links," presented at *OFC*, Anaheim, CA, 2006, and the material in "Modeling of coherent and incoherent Rayleigh crosstalk in conventional optical links," accepted for publication in *Photonic Technology Letters*, July 2007.

The dissertation author was the primary investigator and first author of these publications but would like to thank Dr. Nikola Alic, Dr. Matthias Gross, Prof. George Papen, Prof. Stojan Radic and Prof. Sadik Esener for their helpful suggestions.

2.6 References

[1] M. Abe and R. Takahashi, "Over 1000 channel, 6.25 GHz-spaced ultra-DWDM transmission with supercontinuum multi-carrier source," presented at Optical Fiber Communication Conference, 2005. Technical Digest. OFC/NFOEC, 2005.

[2] H. Suzuki, M. Fujiwara, and K. Iwatsuki, "Application of super-DWDM technologies to terrestrial terabit transmission systems," *Lightwave Technology, Journal of*, vol. 24, pp. 1998-2005, 2006.

[3] P. J. Winzer, M. Pfennigbauer, and R.-J. Essiambre, "Coherent crosstalk in ultradense WDM systems," *Lightwave Technology, Journal of*, vol. 23, pp. 1734-1744, 2005.

[4] L. Paradiso, P. Boffi, L. Marazzi, N. D. Vecchia, M. Artiglia, and M. Martinelli, "Experimental XPM, SPM, FWM penalty evaluation in very dense WDM optical systems," presented at Lasers and Electro-Optics, 2005. (CLEO). Conference on, 2005.

[5] B. Chan and J. Conradi, "On the non-Gaussian noise in erbium-doped fiber amplifiers," *Lightwave Technology, Journal of*, vol. 15, pp. 680-687, 1997.

[6] P. A. Humblet and M. Azizoglu, "On the bit error rate of lightwave systems with optical amplifiers," *Lightwave Technology, Journal of*, vol. 9, pp. 1576-1582, 1991.

[7] D. Marcuse, "Derivation of analytical expressions for the bit-error probability in lightwave systems with optical amplifiers," *Lightwave Technology, Journal of*, vol. 8, pp. 1816-1823, 1990.

[8] E. Desurvire, *Erbium-Doped Fiber Amplifiers*. New York: Wiley, 1994.

[9] N. Alic, G. Papen, R. Saperstein, L. Milstein, and Y. Fainman, "Signal Statistics and Maximum Likelihood Sequence Estimation in Intensity Modulated Fiber Optic Links Containing a Single Optical Pre-amplifier," *Optics Express*, vol. 13, pp. 4568-4579, 2005.

[10] T. Yoshino and G. P. Agrawal, "Photoelectron statistics of solitons corrupted by amplified spontaneous emission," *Physical Review A*, vol. 51, pp. 1662 LP - 1668, 1995.

[11] J. Bromage, P. J. Winzer, and R.-J. Essiambre, "Multiple path interference and its impact on system design," in *Raman Amplifiers for Telecommunciations 2*, M. N. Islam, Ed. New York: Springer-Verlag, 2004, pp. ch. 15.

[12] P. J. Winzer, R.-J. Essiambre, and J. Bromage, "Combined impact of double-Rayleigh backscatter and amplified spontaneous emission on receiver noise," presented at Optical Fiber Communication Conference, 2002.

[13] A. V. Oppenheim, A. S. Willsky, and S. H. Nawab, *Signals and Systems*. Upper Saddle River, N. J.: Prentice Hall, 1997.

[14] M. O. Vandeventer, "Polarization Properties of Rayleigh Backscattering in Single-Mode Fibers," *Journal of Lightwave Technology*, vol. 11, pp. 1895-1899, 1993.

[15] G. Bosco, A. Carena, V. Curri, R. Gaudino, and P. Poggiolini, "On the use of NRZ, RZ, and CSRZ modulation at 40 Gb/s with narrow DWDM channel spacing," *Lightwave Technology, Journal of*, vol. 20, pp. 1694-1704, 2002.

[16] P. J. Winzer, M. Pfennigbauer, M. M. Strasser, and W. R. Leeb, "Optimum filter bandwidths for optically preamplified NRZ receivers," *Journal of Lightwave Technology*, vol. 19, pp. 1263-1273, 2001.

[17] J. L. Rebola and A. V. T. Cartaxo, "Q-factor estimation and impact of spontaneous-spontaneous beat noise on the performance of optically preamplified systems with arbitrary optical filtering," *Lightwave Technology, Journal of*, vol. 21, pp. 87-95, 2003.

[18] M. Pauer, P. J. Winter, and W. R. Leeb, "Bit error probability reduction in direct detection optical receivers using RZ coding," *Lightwave Technology, Journal of*, vol. 19, pp. 1255-1262, 2001.

[19] P. Gysel and R. K. Staubli, "Spectral properties of Rayleigh backscattered light from single-mode fibers caused by a modulated probe signal," *Lightwave Technology, Journal of*, vol. 8, pp. 1792-1798, 1990.

[20] C. R. S. Fludger, Y. Zhu, V. Handerek, and R. J. Mears, "Impact of MPI and modulation format on transmission systems employing distributed Raman amplification," *Electronics Letters*, vol. 37, pp. 970-972, 2001.

[21] C. Martinelli, G. Charlet, L. Pierre, J. Antona, and D. Bayart, "System impairment of double-Rayleigh scattering and dependence on modulation format," presented at Optical Fiber Communications Conference, 2003.

[22] J. Bromage, L. E. Nelson, C. H. Kim, P. J. Winzer, R.-J. Essiambre, and R. M. Jopson, "Relative impact of multiple-path interference and amplified spontaneous emission noise on optical receiver performance," presented at Optical Fiber Communication Conference and Exhibit, 2002. OFC 2002, 2002.

[23] J. W. Goodman, *Statistical Optics*. New York: Wiley & Sons, 1985.

[24] G. Papen and R. Blahut, *Lightwave Communication Systems*, Draft A, Prentice-Hall, 2007.

[25] M. E. V. Valkenburg, *Analog Filter Design*. New York: Holt, Rinehard and Winston, 1982.

[26] M. Pfennigbauer and P. J. Winzer, "Choice of MUX/DEMUX filter characteristics for NRZ, RZ, and CSRZ DWDM systems," *Lightwave Technology, Journal of*, vol. 24, pp. 1689-1696, 2006.

[27] A. Royset and D. R. Hjelme, "Symmetry requirements for 10-Gb/s optical duobinary transmitters," *Photonics Technology Letters, IEEE*, vol. 10, pp. 273-275, 1998.

[28] G. P. Agrawal, *Nonlinear Optics*. San Diego, CA: Elseviar Science, 2001.

[29] M. O. van Deventer and A. J. Boot, "Polarization properties of stimulated Brillouin scattering in single-mode fibers," *Lightwave Technology, Journal of*, vol. 12, pp. 585-590, 1994.

[30] M. O. v. Deventer, *Fundamentals of Bidirectional Transmission Over a Single Optical Fiber*. London: Springer, 1996.

[31] P. Ebrahimi, Y. Wang, A. B. Sahin, L.-S. Yan, A. E. Willner, Y. Qian, and J. Li, "Effects of SBS and Rayleigh scattering in densely-spaced bidirectional transmission using Raman amplification," presented at Lasers and Electro-Optics, 2002. CLEO '02. Technical Digest. Summaries of Papers Presented at the, 2002.

[32] M. O. van Deventer, J. J. G. M. van der Tol, and A. J. Boot, "Power penalties due to Brillouin and Rayleigh scattering in a bidirectional coherent transmission system," *Photonics Technology Letters, IEEE*, vol. 6, pp. 291-294, 1994.

[33] J. M. C. Boggio, J. D. Marconi, and H. L. Fragnito, "Experimental and numerical investigation of the SBS-threshold increase in an optical fiber by applying strain distributions," *Lightwave Technology, Journal of*, vol. 23, pp. 3808-3814, 2005.

[34] A. Consentino and E. Iannone, "SBS threshold dependence on line coding in phase-modulated coherent optical systems," *Electronics Letters*, vol. 25, pp. 1459-1460, 1989.

[35] E. Lichtman, R. G. Waarts, and A. A. Friesem, "Stimulated Brillouin scattering excited by a modulated pump wave in single-mode fibers," *Lightwave Technology, Journal of*, vol. 7, pp. 171-174, 1989.

[36] X. P. Mao, R. W. Tkach, A. R. Chraplyvy, R. M. Jopson, and R. M. Derosier, "Stimulated Brillouin threshold dependence on fiber type and uniformity," *Photonics Technology Letters, IEEE*, vol. 4, pp. 66-69, 1992.

[37] F. W. Willems, W. Muys, and J. S. Leong, "Simultaneous suppression of stimulated Brillouin scattering and interferometric noise in externally modulated lightwave AM-SCM systems," *Photonics Technology Letters, IEEE*, vol. 6, pp. 1476-1478, 1994.

[38] T. Franck, T. N. Nielsen, and A. Stentz, "Experimental verification of SBS suppression by duobinary modulation," presented at Integrated Optics and Optical Fibre Communications, 11th International Conference on, and 23rd

European Conference on Optical Communications (Conf. Publ. No.: 448), 1997.

[39] N. S. Bergano, F. W. Kerfoot, and C. R. Davidson, "Margin Measurements in Optical Amplifier Systems," *Ieee Photonics Technology Letters*, vol. 5, pp. 304-306, 1993.

[40] H. Kim and C. X. Yu, "Optical duobinary transmission system featuring improved receiver sensitivity and reduced optical bandwidth," *Photonics Technology Letters, IEEE*, vol. 14, pp. 1205-1207, 2002.

[41] I. Lyubomirsky and B. Pitchumani, "Impact of optical filtering on duobinary transmission," *Ieee Photonics Technology Letters*, vol. 16, pp. 1969-1971, 2004.